Displacement noise from back scattering and specular reflection of input optics in advanced gravitational wave detectors

B. Canuel,[1,*] **E. Genin,**[1] **G. Vajente,**[2] **and J. Marque**[1]

[1] *European Gravitational Observatory (EGO), I-56021 Cascina (Pi), Italy*
[2] *Istituto Nazionale di Fisica Nucleare (INFN), I-56127 Pisa, Italy*

**benjamin.canuel@ego-gw.it*

Abstract: The second generation of ground-based interferometric gravitational wave detectors are currently being built and installed. They are designed to be better in strain sensitivity by about a factor 10 with respect to the first generation. Light originating from the laser and following unintended paths, called stray light, has been a major problem during the commissioning of all of the first generation detectors. Indeed, stray light carries information about the phase of the emitting object. Therefore, in the next generation all the optics will be suspended in the vacuum in order to mitigate their associated stray light displacement noise. Despite this additional precaution, the challenging target sensitivity at low frequency which is partially limited by quantum radiation pressure combined with up-conversion effects, requires more detailed investigation. In this paper, we turn our attention to stray light originating from auxiliary optical benches. We use a dedicated formalism to compute the re-coupling of back-reflected and back-scattered light. We show, in particular, how much care should be taken in designing and setting requirements for the input bench optics.

OCIS codes: (290.0290) Scattering; (120.3180) Interferometry.

References and links

1. P. G. Nelson, "An analysis of scattered light in reflecting and refracting primary objectives for coronagraphs," Coronal Solar Magnetism Observatory Technical Note 4, http://www.cosmo.ucar.edu/publications/nelson_tech4_10-06.pdf.
2. The LIGO Scientific Collaboration, "LIGO: the laser interferometer gravitational-wave observatory," Rep. Prog. Phys. **72**, 076901 (2009).
3. The Virgo Collaboration, "The Virgo 3 km interferometer for gravitational wave detection," J. Opt. A: Pure Appl. Opt. **10**, (2008).
4. R. Schilling, L. Schnupp, W. Winkler, H. Billing, K. Maischberger, and A. Rudiger, "A method to blot out scattered light effects and its application to a gravitational wave detector," J. Phys. E: Sci. Instrum. **14**(65), (1981).
5. E. Flanagan and K. S. Thorne, "Noise due to backscatter off baffles, the nearby wall and objects at the far end of the beam tube; and recommended actions," LIGO Technical Report, LIGO-T940063-00 (1994).
6. J-Y. Vinet, V. Brisson, and S. Braccini, "Scattered light noise in gravitational wave interferometric detectors: coherent effects," Phys. Rev. D **54**, 1276 (1996).
7. J-Y. Vinet, V. Brisson, S. Braccini, I. Ferrante, L. Pinard, F. Bondu, and E. Tournié, "Scattered light noise in gravitational wave interferometric detectors: a statistical approach," Phys. Rev. D **56**, 6085 (1997).
8. A. Spector and G. Mueller, "Back-reflection from a Cassegrain telescope for space-based interferometric gravitational-wave detectors," Class. Quantum Grav. **29**, 205005 (2012).

#186188 - $15.00 USD Received 28 Feb 2013; revised 5 Apr 2013; accepted 5 Apr 2013; published 23 Apr 2013

9. D. J. Ottaway, P. Fritschel, and S. J. Waldman, "Impact of upconverted scattered light on advanced interferometric gravitational wave detectors," Opt. Express **20**, 8329-8336 (2012), http://dx.doi.org/10.1364/OE.20.008329.
10. S. Hild, "Beyond the first generation: extending the science range of the gravitational wave detector GEO600," PhD Thesis, (2006).
11. The Virgo Collaboration, "Noise studies during the first Virgo science run and after," Class. Quantum Grav. **25**, 184003 (2008).
12. The Virgo Collaboration, "Noise from scattered light in the Virgos second science run data," Class. Quantum Grav. **27**, 194011 (2010).
13. R. Takahashi, K. Arai, S. Kawamura, and M.R. Smith, "Direct measurement of the scattered light effect on the, sensitivity in TAMA300," Phys. Rev. D **70**, 062003 (2004).
14. B. Canuel and E. Genin, "Determination of back scattering and direct reflection recoupling from single optics - application to the end benches," Virgo internal document VIR-0375A-10 (2010), https://tds.ego-gw.it/ql/?c=7570.
15. The Virgo Collaboration, "Advanced Virgo technical design report," Virgo internal document VIR-0128A-12 (2012), https://tds.ego-gw.it/ql/?c=8940.
16. P. Meystre, E. M. Wright, J. D. McCullen, and E. Vignes, "Theory of radiation-pressure-driven interferometers," JOSA B **2**(11), 1830-1840 (1985).
17. G. Muller, T. Delker, D. B. Tanner, and D. Reitze, "Dual-recycled cavity-enhanced Michelson interferometer for gravitational-wave detection," Appl. Opt. **42**, 1257 (2003).
18. The Virgo Collaboration, "Laser with an in-loop relative frequency stability of 1.0×10^{-21} on a 100-ms time scale for gravitational-wave detection," Physical Review A **79**, 053824 (2009).
19. S. Hild, H. Grote, J. Degallaix, S. Chelkowski, K. Danzmann, A. Freise, M. Hewitson, J. Hough, H. Lück, M. Prijatelj, K. A. Strain, J. R. Smith, and B. Willke, "DC-readout of a signal-recycled gravitational wave detector," Class. Quantum Grav. **26**, 055012 (2009).
20. E. Tournefier, "Back-scattering by the optical benches: results from Virgo and constraints for AdV," Virgo internal document VIR-0070A-08 (2008), https://tds.ego-gw.it/ql/?c=2083.
21. B. Canuel, I. Fiori, J. Marque, and E. Tournefier, "Diffused light mitigation in Virgo and constraints for Virgo+ and AdV," Virgo internal document VIR-0792A-09 (2009), https://tds.ego-gw.it/ql/?c=7118.
22. Optickle home-page, http://ilog.ligo-wa.caltech.edu:7285/advligo/ISC_Modeling_Software.
23. M. Smith, "Baffling requirements for the 4K and 2K IFO," working note of the LIGO Project, LIGO-T980027-00 (1998).
24. M. Barsuglia, C. Buy, B. Canuel, R. Day, E. Genin, and G. Vajente, "AdV INJ: mode matching telescope configuration choice for the ITF input telescope," Virgo internal document VIR-0010A-12 (2011) https://tds.ego-gw.it/ql/?c=8812.
25. J. C. Stover, "Optical scattering measurement and analysis," SPIE Press, Bellingham, WA, 2nd Edition (1995).
26. E. L. Church, "Fractal surface finish," Appl. Opt. **27**, 1518-1526 (1988), http://dx.doi.org/10.1364/AO.38.002870.
27. C. J. Walsh, A. J. Leistner, and B. F. Oreb, "Power spectral density analysis of optical substrates for gravitational-wave interferometry," Appl. Opt. **38**, 4790-4801 (1999) http://dx.doi.org/10.1364/AO.38.004790.
28. C. J. Walsh, A. J. Leistner, J. Secko, B. F. Oreb, and D. I. Farrant, "Fabrication and measurement of optics for the laser interferometer gravitational wave observatory," Appl. Opt. **38**, 2870-2879 (1999), http://dx.doi.org/10.1364/AO.38.002870.
29. A. Duparré, J. Ferre-Borrull, S. Gliech, G. Notni, J. Steinert, and J. M. Bennett, "Surface characterization techniques for determining the root-mean-square roughness and power spectral densities of optical components," Appl. Opt. **41**, 154-171 (2002) http://dx.doi.org/10.1364/AO.41.000154.
30. The Virgo collaboration, "Characterization of the Virgo seismic environment," Class. Quantum Grav. **29**, 025005 (2012).
31. G. Losurdo et al., "Inertial control of the mirror suspensions of the VIRGO interferometer for gravitational wave detection," Rev. Sci. Instrum. **72**, 3653 (2001).
32. The Virgo collaboration, "Virgo: a laser interferometer to detect gravitational waves," Journal of Instrumentation **7**, P03012 (2012).

1. Introduction

Stray light may affect the performances of many optical systems. Such kind of issue often originates from electro-magnetic radiation external from the system itself. But, in some cases, the stray light is simply the light from the source of the system itself that is following a different path from the intended one. This can happen through various processes: residual reflection from anti-reflective coatings, scattering from imperfect mirror surfaces, scattering from surface defects (like dust, digs or scratches), scattering from the enclosure of the optical system, and

#186188 - $15.00 USD Received 28 Feb 2013; revised 5 Apr 2013; accepted 5 Apr 2013; published 23 Apr 2013

diffraction from the limited aperture of the optics. These processes can actually play a major role and need to be taken into account when designing demanding optical systems such as instruments for astronomy [1] or interferometers for Gravitational Wave (GW) detection [2, 3].

Stray light in GW detectors has long been identified as a serious issue [4] and was taken into account in the design of the first generation of GW interferometers [5–7], but it remains a major concern for the Laser Interferometer Space Antenna [8], as well as for the second generation of ground based interferometers [9].

Indeed, all first generation GW interferometers have experienced problems during their commissioning phase [10]. By carrying out specific measurements, many of these issues have been identified as originating from the scattering or even the specular reflection of some optics at different ports of the interferometers [11–13]. To fix these issues, it was fundamental to calculate the amount of light re-coupling to the main interferometer laser beam from each single optic [14]. Besides, while the first generation stray light displacement noise was critical through the phase modulation of the stray light, the second generation will suffer more severe constraints also through the amplitude modulation of the stray light due to the radiation pressure effects as pointed out in [9]. In the same reference, the effect of noise up-conversion is underlined when high microseismic conditions are taken into account, setting even more stringent requirements. It is then crucial to calculate accurately the light which re-couples to the interferometer for every single optical element in order to set its optical requirements or even make important optical setup design choices.

In this paper we will present a complete formalism to calculate the amount of light that is scattered or reflected once by an optic and directly re-couples to the interferometer. The formalism does not apply in case of multiple scattering events: for this specific case, a detailed study can be fond in [5] for instance. This re-coupling depends on which port of the interferometer the considered element is installed in. It also depends on the geometrical re-coupling of the back-reflected light on the fundamental mode of the interferometer. The same is true also for the back-scattered light. This last contribution is particularly problematic to quantify as we lack a simple model. We will present also which parameters to take into account and how to calculate how the scatterer motion translates into displacement noise at the interferometer output. As the most critical elements will be those placed at normal incidence, we expect the lenses of the input and output mode matching telescopes of Advanced Virgo [15], which consist of a meniscus lens and two parabolic mirrors, to be particularly critical. We will therefore apply the formalism to calculate the displacement noise produced by the meniscus lens of the input mode matching telescope of Advanced Virgo, and discuss about its relevant optical requirements. Of course, the treatment presented in this article is general and the method may be applied to any component of the optical setup of the auxiliary optics of the interferometer, in order to check if its optical specification and seismic isolation are compliant or not with the target science sensitivity.

2. Recoupling of stray light emitted from the external benches-Formalism

2.1. Coupling mechanism of stray light

The laser light which exits from one of the output ports of an interferometer will travel through several optical elements. These elements can couple back some light into the interferometer port due to back reflection or scattering. This back propagating light enters into the instrument and can recouple with the main mode, adding a spurious field to the main one. This field will be in general not constant, but it will contain phase and amplitude information linked to the optical element motion. Since the amount of stray light is typically very small, the additional

#186188 - $15.00 USD Received 28 Feb 2013; revised 5 Apr 2013; accepted 5 Apr 2013; published 23 Apr 2013

noise to strain amplitude h will depend linearly on the amplitude of the field and we can write:

$$h = \sqrt{f_r} G\left(\frac{z_r}{\lambda}\right) \tag{1}$$

where f_r is the fraction of the light power exiting one of the interferometer ports which is coupled back into the main mode and z_r is the position of the reflecting object. It is not possible in general to assume that the object motion is small and therefore the coupling function G is not linear in the displacement z_r. To properly evaluate the impact of stray light to the detector sensitivity it is therefore necessary to compute the fraction f_r and to fully understand the coupling function G, including non-linear effects. In this section we describe how to characterize G, while in the following ones we show a way to compute f_r in the case of specular reflection (f_{sp}) and diffusion (f_{sc}).

In the following, we will note E_{in} the field inside the interferometer, at a reference point which is relevant to compute the coupling of additional stray light to the detector sensitivity. E_{out} is the field exiting from one of the interferometer ports at the location of the stray light source. E_r is the part of this field which is scattered or reflected back and recoupled with the main interferometer mode at the reference point where E_{in} is computed.

The motion z_r of the stray light source will be encoded in the phase of the recoupled field E_r

$$\phi_r(t) = \frac{4\pi}{\lambda} z_r(t) \tag{2}$$

The motion of the stray light source can span over multiple wavelengths, therefore the phase can be large and wrapping many times around 2π. This introduces a large non linear behavior of the stray light noise coupling.

E_r will sum to the unperturbed field inside the interferometer E_{in}:

$$E_{in} + E_r = E_{in} + \sqrt{f_r} E_{out} e^{i\phi_0 + i\phi_r(t)} \tag{3}$$

where ϕ_0 is a static phase which depends on the scattered position in the interferometer. If we are considering the input port of the interferometer, the E_{in} field can be identified with the one corresponding to the input beam. When considering other ports which are not used to inject the main beam into the detector, one should carefully compute the coupling of the back-propagating field with the main one inside the interferometer. In this case the f_r term must take into account the propagation of the field to the reference position inside the instrument. In both cases, the net effect is an additional phase and amplitude modulation of the interferometer field:

$$E_{in} + E_r = E_{in}\left(1 + \sqrt{f_r}\frac{E_{out}}{E_{in}} e^{i\phi_0 + i\phi_r(t)}\right) \tag{4}$$

The ratio of the two field amplitude is given by the square root of the ratio of the powers plus an additional phase which can be included in ϕ_0:

$$\begin{aligned} E_{in} + E_r &= E_{in}\left(1 + \sqrt{f_r \frac{P_{out}}{P_{in}}} e^{i\phi_0 + i\phi_r(t)}\right) & (5) \\ &= E_{in} \exp\left[\sqrt{f_r \frac{P_{out}}{P_{in}}} \left(\cos(\phi_0 + \phi_r(t)) + i\sin(\phi_0 + \phi_r(t))\right)\right] & (6) \end{aligned}$$

where to derive the second equality we considered that $f_r \frac{P_{out}}{P_{in}}$ is much smaller than unity and considered that at first order $1 + x \simeq e^x$. Moreover, the exponential term depending on the phases has been splitted in the real and imaginary part. The dominant noise coupling can be phase or

#186188 - $15.00 USD Received 28 Feb 2013; revised 5 Apr 2013; accepted 5 Apr 2013; published 23 Apr 2013

amplitude, depending on the static phase ϕ_0, or in other words depending on the microscopic position of the stay light source relative to the interferometer. If the motion of the scattering element is much larger than one wave-length, the distinction between ϕ_0 and $\phi_r(t)$ is irrelevant and the noise coupling will proceed through both phase and amplitude.

The effect of stray light is therefore described by additional phase and amplitude noises at the interferometer considered port given by

$$n_\phi(t) = \sqrt{\frac{f_r P_{out}}{P_{in}}} \sin(\phi_0 + \phi_r(t)) \tag{7}$$

$$\frac{\delta P(t)}{P} = \sqrt{\frac{f_r P_{out}}{P_{in}}} \cos(\phi_0 + \phi_r(t)) \tag{8}$$

These additional noises have amplitudes proportional to $\sqrt{f_r}$ and therefore they can be considered as small perturbations to the circulating field. The non-linear behavior of the coupling function G is completely encoded in the above equations, that can be used to compute the phase and amplitude noise that enters the interferometer at the considered port. The noise can then be propagated to the detector sensitivity using the linear response of the system to additional phase and amplitude noise sources placed at the reference position. In the worst case scenario the contribution of each of the two noise sources to the sensitivity is given by

$$\tilde{h}(f) = T(f) \sqrt{\frac{f_r P_{out}}{P_{in}}} \mathscr{F}[\cos(\phi_r(t))] \tag{9}$$

where $\tilde{h}(f)$ is the amplitude spectrum of the noise as measured in the sensitivity, $\mathscr{F}$ indicates the Fourier transform and $T(f)$ is the linear response of the interferometer to phase or amplitude noise.

The interferometer transfer functions $T(f)$ depend strongly on the optical configuration of the system. In particular, advanced gravitational wave interferometers are very sensitive to all asymmetries between the two arms: mirror radii of curvature, round trip losses and Fabry-Perot cavity finesse. Moreover, advanced detectors will feature a large amount of stored power (800 kW inside the km-long arm cavities) that will introduce significant radiation pressure effects: any field fluctuation can induce a force on the test masses, which significantly change the detector response [16]. For all these reasons it is mandatory to use detailed optical simulations to compute the response of the interferometer to phase and amplitude noise. An example for an interferometer with Advanced Virgo like parameters is given in Fig. 1. Moreover, the noise entering from some of the interferometer ports might be affected by the action of the feed-back control systems that are needed to actively maintain the detector at its working point. In the following sections of this paper we will focus our attention on stray light coming from the main input port of the interferometer. In this case the phase noise introduced by any stray light source will be suppressed by the frequency stabilization control [18] and the dominant contribution will be the amplitude noise. Indeed advanced detectors will implement a DC readout scheme [19], which is particularly sensitive to amplitude noise at the input.

In the commissioning of first generation detectors the main coupling path was through phase modulation of the main interferometer field. Therefore the G function was considered to be simply [12]

$$G = k \sin\left(\frac{4\pi}{\lambda} z_r\right) \tag{10}$$

where k was assumed to be a frequency independent coefficient describing the coupling of the back propagating field with the main one. This model worked well in the case of Virgo and Virgo+ [12, 20, 21]. In the case of Advanced Virgo, stray light noise will be characterized by

#186188 - $15.00 USD Received 28 Feb 2013; revised 5 Apr 2013; accepted 5 Apr 2013; published 23 Apr 2013

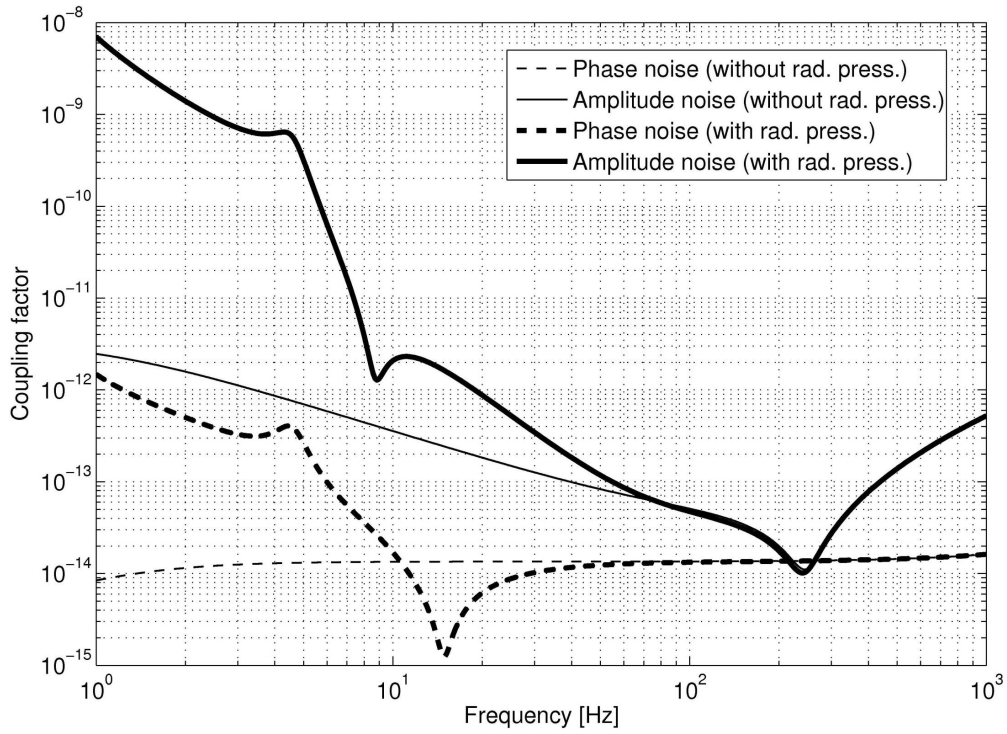

Fig. 1. Coupling to the detector sensitivity of phase and amplitude noises at the input of an interferometer with Advanced Virgo like parameters. These curves have been computed using an optical simulation of the dual recycled interferometer. For more details please refer to [15] and [17]. The thin curves refers to the (unphysical) case that neglects radiation pressure effects. Thick curves instead shows the simulation outcome in the more realistic case. The couplings are given for $f_r = 1$. The sensitivity is expressed in adimensional strain h.

the frequency dependent coupling factors $T(f)\sqrt{\frac{f_r P_{out}}{P_{in}}}$ for both amplitude and phase noises. We computed these factors using a simulation based on Optickle [22] and the results are shown in Fig. 1 supposing $f_r = 1$. The unphysical case of no radiation pressure effects is also shown for comparison. We observe that these effects play a major role for frequencies below 100 Hz. In order to project displacement noise of a stray light source on detector sensitivity, we need to calculate the fraction of the light power f_r which is coupled back into the main mode. In the following sections, we carry out the calculation both for scattered light f_{sc} and specular reflection f_{sp}.

2.2. Calculation of scattered light recoupling f_{sc}

In this section, we explain how to calculate the fraction of scattered light f_{sc} recoupled to the main mode of the interferometer starting from the BRDF (Bidirectional Reflectance Distribution Function) of the diffusing optic considered. Scattered photons from the optics placed on the external benches are propagated inside the interferometer using geometrical optics and recoupling is then calculated by numerical integration.

#186188 - $15.00 USD Received 28 Feb 2013; revised 5 Apr 2013; accepted 5 Apr 2013; published 23 Apr 2013

2.2.1. f_{sc} as a function of surface BRDFs

A single photon scattered from the diffusing surface can be described by its emitting position (r,α) and its normalized emitting direction $(\phi\cos\theta, \phi\sin\theta, 1)$ (see Fig. 2).

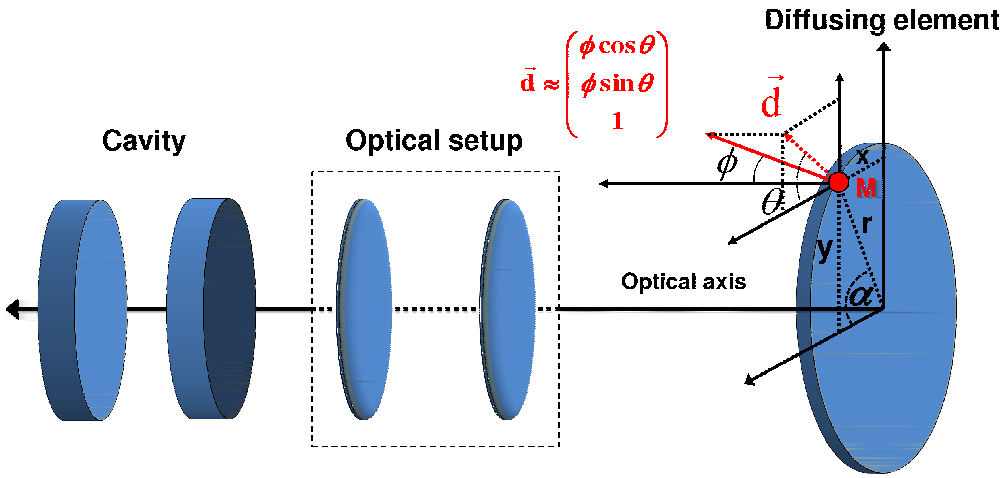

Fig. 2. A photon can be described by its emitting point M and normalized direction d.

Considering an radial symmetry around the optical axis, we define the boolean recoupling function $F(r,\theta,\phi)$ which is equal to 1 if the photon is recoupled, 0 otherwise. The power recoupled from an element of surface dS of the diffusing object can be written:

$$d^2P = \int_0^{2\pi}\int_0^{\pi/2} \frac{dP}{d\Omega}\sin(\phi)F(r,\theta,\phi)\mathrm{d}\theta\mathrm{d}\phi \tag{11}$$

where

$$\frac{dP}{d\Omega} = d^2P_i\cos(\phi)\mathrm{BRDF}(r,\phi) \tag{12}$$

where P_i is the power incident on the surface dS: $d^2Pi = rI(r)\mathrm{d}\alpha\mathrm{d}r$. The total power recoupled P is obtained by integration over the whole surface:

$$P = \int_0^{\infty}\int_0^{2\pi}\int_0^{\frac{\pi}{2}} 2\pi rI(r)\cos\phi\sin\phi\mathrm{BRDF}(r,\phi)F(r,\theta,\phi)\mathrm{d}r\mathrm{d}\theta\mathrm{d}\phi \tag{13}$$

where the factor 2π comes from integration over α, given the radial symmetry. f_{sc} is then obtained by the ratio P over the incoming power P_0:

$$f_{sc} = \frac{P}{P_0} \tag{14}$$

2.2.2. Calculation of the recoupling function.

In this section we explain how to calculate $F(r,\theta,\phi)$. To do this, we carry out the propagation of the photon inside the optical system placed on the external bench. Then the photon is propagated through the interferometer cavities. The photon is considered resonant if it couples with both systems. It means that it should not go outside the different optical apertures.

In the case of the cavity propagation, the photon should make a number of round trips of about $F/2\pi$, where F is the cavity Finesse, without going outside the mirror coatings. As the

#186188 - $15.00 USD Received 28 Feb 2013; revised 5 Apr 2013; accepted 5 Apr 2013; published 23 Apr 2013

coating size is set to about 6 times the Gaussian beam radius on the considered mirror, this criteria guarantees that the photon remains within the cavity mode. All the photons verifying this criteria are then considered to interfere constructively with the cavity field which represents the worst possible case. The sum of all these photons (given by Eq. (13)) may create a field that has the right phase and spatial distribution to re-couple in the most efficient way inside the interferometer. The quantity f_{sc} therefore provides an upper limit of the recoupling.

In order to check if a given photon emitted by the scattering surface (that we suppose here placed perpendicularly to the beam propagation, which is the worst case) superates the above criteria, we calculate its coordinates x_i, y_i, z_i in the plane of the optical component number i using geometrical optics and check if $(x_i^2 + y_i^2)^{\frac{1}{2}} < a_i$ where a_i is the radius of this component.

More into details, a photon at any instant of its propagation can be described by its position and direction summarized in the 6-vector:

$$u(x,y,z,\theta,\phi) = \begin{pmatrix} x \\ y \\ z \\ \phi\cos(\theta) \\ \phi\sin(\theta) \\ 1 \end{pmatrix} \tag{15}$$

It can be easily shown that the propagation matrix of a free-space distance d, and the propagation matrix through a thin lens of focal f, respectively named $P(d)$ and $L(f)$ can be written:

$$P(d) = \begin{pmatrix} 1 & 0 & 0 & d & 0 & 0 \\ 0 & 1 & 0 & 0 & d & 0 \\ 0 & 0 & 1 & 0 & 0 & d \\ 0 & 0 & 0 & 1 & 0 & 0 \\ 0 & 0 & 0 & 0 & 1 & 0 \\ 0 & 0 & 0 & 0 & 0 & 1 \end{pmatrix} \quad L(f) = \begin{pmatrix} 1 & 0 & 0 & 0 & 0 & 0 \\ 0 & 1 & 0 & 0 & 0 & 0 \\ 0 & 0 & 1 & 0 & 0 & 0 \\ -\frac{1}{f} & 0 & 0 & 1 & 0 & 0 \\ 0 & -\frac{1}{f} & 0 & 0 & 1 & 0 \\ 0 & 0 & 0 & 0 & 0 & 1 \end{pmatrix} \tag{16}$$

The optical system may be described as a succession of elementary matrices M_i of type L or P. These matrices enable a fast calculation of the full propagation matrix R_i on the element i. $R_i = \prod_{j=1}^{i} M_i = M_i R_{i-1}$. Then we have:

$$F(r,\theta,\phi) = \| R_1.u_0(r,0,0,\theta,\phi) \| < a_1 \ldots \wedge \| R_k.u_0(r,0,0,\theta,\phi) \| < a_k \tag{17}$$

where a_i is the optical aperture of element i, u_0 the vector representing photons emitted by the diffusing surface and where the norm corresponds to the distance of the photon from the optical axis:

$$\| u(x,y,z,\theta,\phi) \| = (x_i^2 + y_i^2)^{\frac{1}{2}} \tag{18}$$

Knowing the BRDF of the diffusing surface and the recoupling function $F(r,\theta,\phi)$, the fraction of scattered light f_{sc} recoupled to the main mode of the interferometer is calculated using Eq. (13) and Monte-Carlo numerical integration.

2.2.3. Example of calculation using AdV cavities

As said before, the recoupling f_{sc} obviously depends on the optical setup of the input or output optics, the geometry of the interferometer cavity and the BRDF of the optic considered. In order to draw some general consideration on the parameters influencing the recoupling, we consider here a simplified case presented in Fig. 3.

In this case, we calculate the quantity of light emitted by a diffusing element (Total Integrated Scatter, TIS=1) placed on the symmetric port of the interferometer (ITF), before the recycling

#186188 - $15.00 USD Received 28 Feb 2013; revised 5 Apr 2013; accepted 5 Apr 2013; published 23 Apr 2013

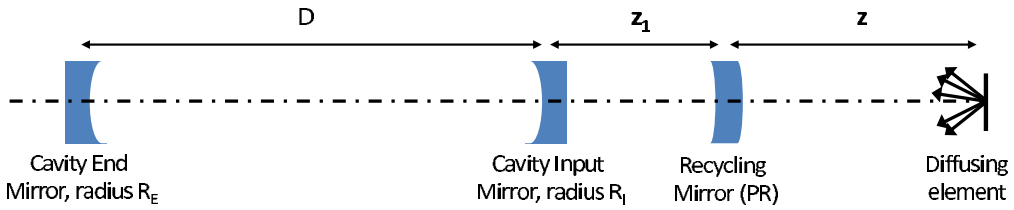

Fig. 3. Setup considered for calculating the recoupling of a diffusing element placed on the symmetric port of the interferometer, at a variable distance from the recycling mirror. Optical parameters are those of AdV.

mirror. We will suppose here that the surface is Lambertian, which means it has a constant BRDF. This is a realistic supposition for all optics tilted by a macroscopic angle (about 5-10°) such as most of the mirrors or photodiodes. Indeed, in such cases, only large angle scattering will contribute to cavity recoupling. In the case considered here: TIS=1, we have BRDF=$1/\pi$. Using formalism presented in the previous paragraph, we derive in table 1 the propagation matrix of a single photon emitted by the diffusing surface on ith surface.

Table 1. Calculation of the propagation matrixes R_i for a photon emitted from a diffusing element placed before the PR mirror. f_{tPR} and f_{tIN} are the focal in transmission of the PR and input mirrors.

Propagation matrix R_i	Propagation on:
$R_1 = P(z)$	PR
$R_2 = P(z_1).L(f_{tPR}).R_1$	Input Mirror
$R_3 = P(D).L(f_{tIN}).R_2$	End Mirror
... for n$\geq$ 1	
$R_{2n+2} = P(D).L(R_E/2).R_{2(n-1)+3}$	Input mirror
$R_{2n+3} = P(D).L(R_I/2).R_{2(n-1)+4}$	End mirror

Using R_i matrixes and the relative optical apertures, it is possible to obtain the function $F(r,\theta,\phi)$ using Eq. (17) and then to calculate f_{sc}. Figure 4 shows the value of f_{sc} as a function of distance of the diffusing object with respect to the PR mirror.

We observe that the recoupling varies of a few orders of magnitude as a function of distance to PR mirror and reaches a maximum at waist location.

From this simplified example, we see that much care should be used on the external benches to place the most diffusing optics far from the waist location in order to lower recoupling. Furthermore, optical designs with small beam waists should be avoided. Indeed, the recoupling at the waist location can be approximated by the multiplication of the solid angle of the beam aperture with the BRDF [23]:

$$f_{sc} \approx \frac{\mathrm{BRDF}\lambda^2}{\pi\omega_0^2} = \frac{\lambda^2}{\pi^2\omega_0^2} \tag{19}$$

which clearly demonstrate a $1/\omega_0^2$ dependance. Considerations derived from this example are in fact very general and apply to the whole optical setup of the external benches. Of course, discussion is carried out here considering a constant BRDF and treatment of optics placed perpendicularly to the optical axis, such as lenses, should be done considering their exact PSDs. Indeed, such elements may become critical and a dedicated example will be given in section 3 in the case of the injection (INJ) mode matching telescope.

#186188 - $15.00 USD Received 28 Feb 2013; revised 5 Apr 2013; accepted 5 Apr 2013; published 23 Apr 2013

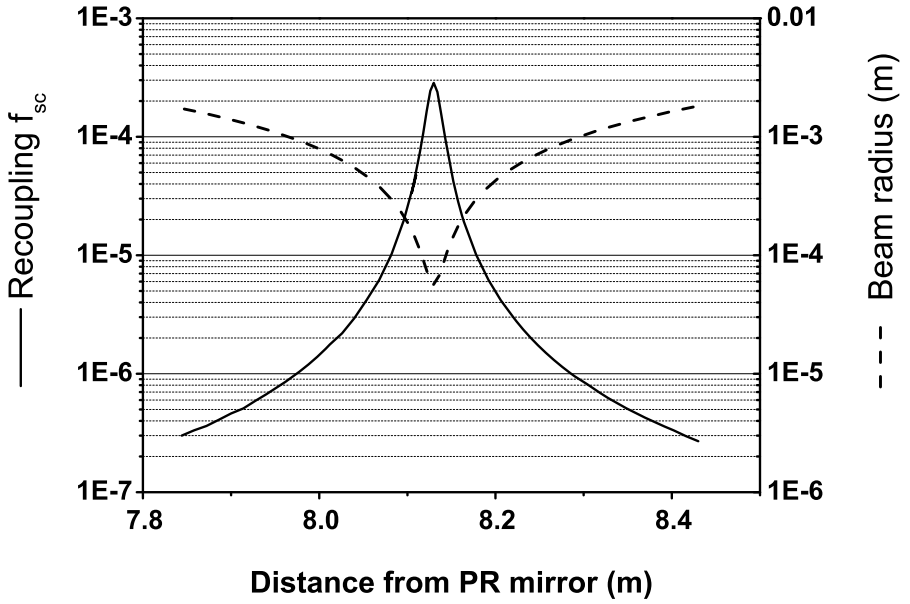

Fig. 4. f_{sc} (black, left scale) as a function of distance of the diffusing object with respect to the PR mirror. Beam radius as a function of distance to PR (dotted line, right scale) is also displayed as reference.

2.3. Recoupling from reflection f_{sp}

Light back reflected towards the interferometer by specular reflection may also recouple to the interferometer mode and generate noise on dark fringe signal by the mechanisms explained in section 2.1. The fraction of recoupled light f_{sp} from an optical element with reflectivity α is given by the overlap integral:

$$f_{sp} = \alpha |\langle \varphi_R | \varphi_i \rangle|^2 \tag{20}$$

where φ_i and φ_R are respectively the incoming and reflected laser fields. We consider the situation described in Fig. 5 where the incoming beam has a Rayleigh range $z_0 = \pi\omega_0^2/\lambda$ and the reflecting element is placed at a distance D from the waist position. As the reflecting element can be for example a lens, we consider that the surface has a curvature R and is slightly tilted with respect to the optical axis by an angle β. Equation (20) can be computed analytically assuming the input mode is a pure gaussian beam:

$$f_{sp} = \frac{\alpha R^2 z_o^2 \exp\left[-\frac{2\pi D^2 z_0 \beta^2}{2\lambda}\left(\frac{1}{D^2+z_0^2}+\frac{1}{(D-R)^2+z_0^2}\right)\right]}{(D^2+z_0^2)[(D-R)^2+z_0^2]} \tag{21}$$

In this section we have seen a complete formalism to calculate noise coupling on the dark fringe of the displacement noise created by specular reflection or scattering of the optics placed on the external benches. As we expect the most critical elements will be those placed perpendicular to the optical axis, we will study in the following the particular case of the Meniscus lens of the mode matching telescope, which is an element placed just before the recycling mirror of the AdV interferometer.

#186188 - $15.00 USD Received 28 Feb 2013; revised 5 Apr 2013; accepted 5 Apr 2013; published 23 Apr 2013

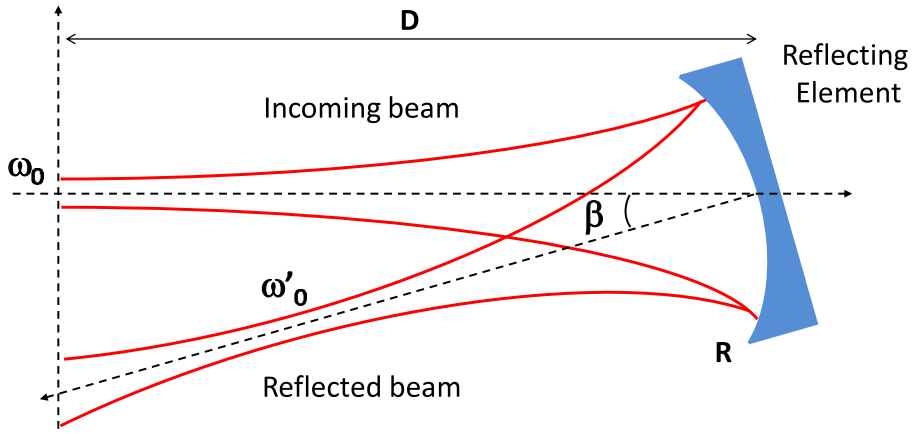

Fig. 5. A reflected element of curvature R is located at a distance D from the incoming beam waist position and is tilted with an angle β.

3. Application to Interferometer mode matching telescope of AdV.

The choice of a marginally stable recycling cavity configuration for Advanced Virgo [15] required the development of a very compact mode matching telescope with a large magnification: around 19 for the whole interferometer mode matching telescope since the beam radius has to be increased from 2.6mm up to 49mm. As no large optics could be placed on the suspended injection bench, this implied to achieve part of the magnification using a curved anti-reflective surface for the Power Recycling mirror. The setup chosen is detailed in Fig. 6. It consists of an afocal off-axis parabolic telescope made of 2 mirrors (PM_1 and PM_2). Then a diverging lens

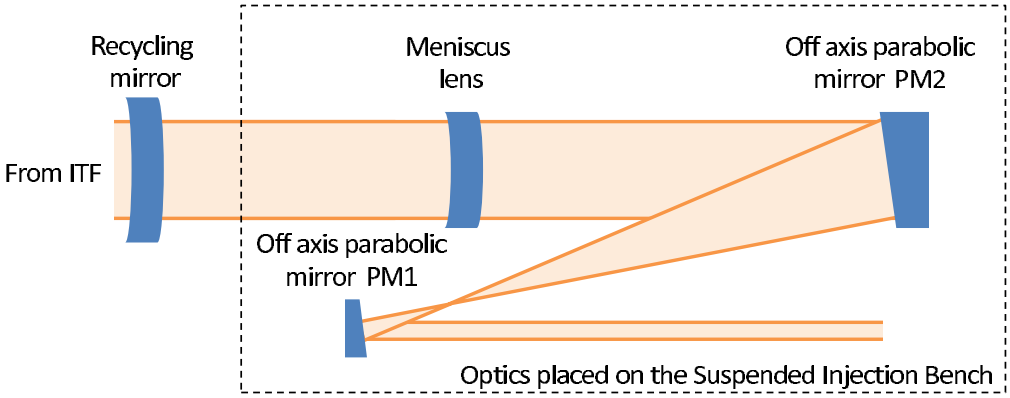

Fig. 6. Overview of the catadioptric telescope.

(meniscus lens) is used in combination with the PR mirror to obtain an interferometer matching as good as 99.9% [24]. One of the main concerns of this configuration is that the meniscus lens is placed perpendicular to the laser beam and may be an important source of stray light that can spoil the interferometer sensitivity [11]. The polishing quality as well as the low reflectivity of this optic are therefore major issues. This will be studied in this section calculating the coupling factors by diffusion and reflection of the meniscus, and projecting the associated noise on the interferometer sensitivity using the formalism presented in section 2.

#186188 - $15.00 USD Received 28 Feb 2013; revised 5 Apr 2013; accepted 5 Apr 2013; published 23 Apr 2013

3.1. *Coupling factor f_{sc} for diffused light of the Meniscus*

In order to calculate the recoupling f_{sc} of the Meniscus using Eq. (13), we need to know the BRDF of the surface which will be determined in the following from the polishing specifications.

The BRDF of an optical surface illuminated at normal incidence can be expressed from its Power Spectral Density (PSD) by [25]:

$$\mathrm{BRDF}(f_x, f_y) = \frac{16\pi^2}{\lambda^4}\cos\phi\,\mathrm{PSD}(f_x, f_y) \tag{22}$$

where f_x and f_y are the spacial frequencies of the surface roughness in cartesian coordinates. In the following, we will consider that the surface has an isotropic roughness and therefore, the function PSD(f_x,f_y) has a radial symmetry. The PSD can be therefore expressed in polar coordinates (f,γ), with $f = \sqrt{f_x^2 + f_y^2}$ and $\gamma = \arctan(f_y/f_x)$. It is then common [25] to work with a simplified isotropic PSD (PSD_{ISO}) obtained by integration over γ:

$$\mathrm{PSD}_{ISO}(f) = \int_0^{2\pi} \mathrm{PSD}(f,\gamma)\,f\,\mathrm{d}\gamma = 2\pi f\,\mathrm{PSD}(f,\gamma) \tag{23}$$

The BRDF of the surface can then be expressed as:

$$\mathrm{BRDF}(f,\gamma) = \mathrm{BRDF}(f) = \frac{16\pi^2}{\lambda^4}\cos\phi\,\frac{1}{2\pi f}\mathrm{PSD}_{ISO}(f) \tag{24}$$

In order to reduce scattering issues, superpolishing will be required for this optical component. As shown by Church [26], highly finished optical surfaces can be described by fractal models and their Power Spectral Densities expressed by an inverse power-law of the form:

$$\mathrm{PSD}_{\mathrm{ISO}}(f) = \frac{K}{f^n} \tag{25}$$

The value of n for Fused Silica is found in the literature to range from 1 to 1.5 [26–29] while K can be determined by integration over all surface spatial frequencies and expressed as a function of total surface roughness σ [25]:

$$\int \mathrm{PSD}_{\mathrm{ISO}}(f)\mathrm{d}f = \sigma^2 \tag{26}$$

Using the PSD model given by Eq. (25), the BRDF can be expressed:

$$\mathrm{BRDF}(f) = \frac{8\pi}{\lambda^4}\cos\phi\,\frac{K}{f^{n+1}} \tag{27}$$

As a single spacial frequency f will create a scattering at a single angle ϕ ,with $f = \sin\phi/\lambda$, the BRDF can therefore be expressed as a function of scattering angle ϕ:

$$\mathrm{BRDF}(\phi) = 8\pi\cos\phi\,\lambda^{n-3}\frac{K}{\sin^{n+1}\phi} \tag{28}$$

Finally the BRDF of a curved surface will depend on its radius of curvature R and may be obtained by a variable change:

$$\mathrm{BRDF}(r,\phi) = \mathrm{BRDF}\left(\phi - 2\arcsin\left[\frac{r}{R}\right]\right) \tag{29}$$

#186188 - $15.00 USD Received 28 Feb 2013; revised 5 Apr 2013; accepted 5 Apr 2013; published 23 Apr 2013

The BRDF in this particular case depends on the distance from the optical axis r. Using the optical setup presented in Fig. 6 and the BRDF model given by Eq. (29), we carried out the calculation of scattered light recoupling of the meniscus f_{sc}. As the spectral index n is not a-priori known and will depends on the polisher, calculations were carried out for different values of n between 1 and 1.5. Supposing that the surface will present a total roughness σ of 10 nm RMS, we derive the spectral strength K for each value of n using Eq. (26).

Results for the two surfaces of the meniscus lens (of radius R_1= -1.07 m and R_2= -3.195 m) are given in table 2 supposing the use of an anti-reflection coating of 100 ppm. We observe that f_{sc} hardly depends on the spectral index n.

Table 2. Scattered light recoupling f_{sc} of the meniscus faces for different spectral index supposing the use of an anti-reflection coating of 100ppm.

Spectral index n	f_{sc} first face	f_{sc} second face
1	$1.8\ 10^{-12}$	$1.5\ 10^{-11}$
1.1	$1.8\ 10^{-12}$	$1.4\ 10^{-11}$
1.2	$1.7\ 10^{-12}$	$1.3\ 10^{-11}$
1.3	$1.6\ 10^{-12}$	$1.3\ 10^{-11}$
1.4	$1.5\ 10^{-12}$	$1.2\ 10^{-11}$
1.5	$1.4\ 10^{-12}$	$1.1\ 10^{-11}$

3.2. *Coupling factor f_{sp} for back-reflected light of the Meniscus*

The other important aspect to be studied is the amount of back-reflected light f_{sp} coming from the meniscus lens surfaces that is recoupled into the interferometer. In order to compute f_{sp}, we determined the parameters (waist size and position) of the beam incident on the 2 surfaces of the meniscus lens and we used Eq. (21). Figure 7 shows the parameters considered in this computation. The beam coming from the interferometer (black line of Fig. 7) has a waist ω_{01}

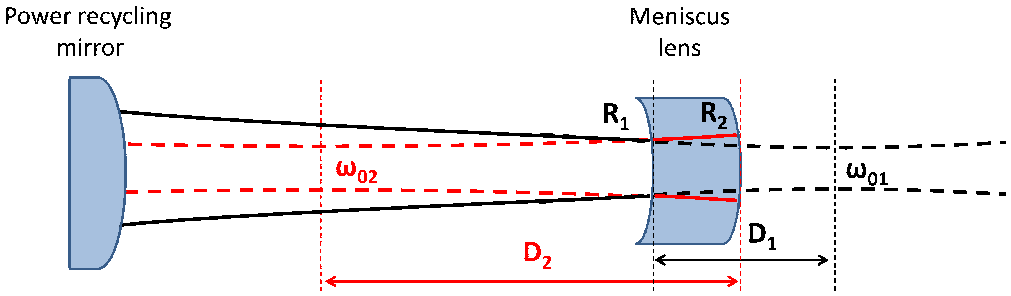

Fig. 7. Coupling of meniscus lens faces back-reflected beams.

located at D_1 from the meniscus lens surface 1. Reflection of this beam on the first surface of the meniscus recombines with the interferometer with a coupling factor f_{sp1}. Transmission through the first surface of the meniscus lens then creates a beam of waist ω_{02} located at D_2 from the second surface. Reflection of this beam on the second surface of the meniscus lens may recombine to the interferometer main beam with a coupling factor f_{sp2}. Beam parameters used for calculation of f_{sp1} and f_{sp2} were computed using Zemax and are given in table 3.

Considering that the reflectivity of the meniscus surfaces is only 100ppm (what we can expect from a good anti-reflective coating), we obtain for a perfectly aligned optic ($\beta = 0$)

#186188 - $15.00 USD Received 28 Feb 2013; revised 5 Apr 2013; accepted 5 Apr 2013; published 23 Apr 2013

Table 3. Parameters considered for the computation of recoupling of back reflected light from meniscus lens surfaces.

Meniscus lens face	Waist size (μm)	Waist position (m)	Radius of curvature (m)	AR coating reflectivity
Face 1	ω_{01}=56	D_1=3.588	R_1=1.072	α_1=100ppm
Face 2	ω_{02}=110.5	D_2=10.273	R_2=3.195	α_2=100ppm

f_{sp1}=3.5.10^{-11} and f_{sp2}=5.2.10^{-10}.

Since in reality there is a small error on optical alignment, it may be interesting to study the variation of f_{sp1} and f_{sp2} with β which is shown on Fig. 8. We observe that f_{sp2} drops quickly

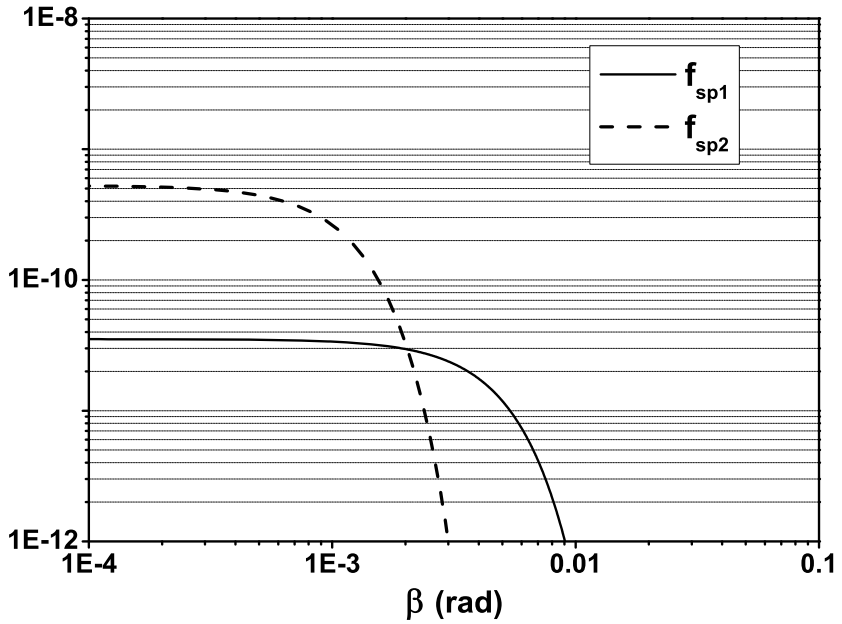

Fig. 8. Variation of recoupling of reflected light by the two faces of the meniscus as a function of its misalignment β.

when the misalignment is around 1 mrad. The difference between the f_{sp1} and f_{sp2} curves is due to the size of the waist reflected by the two surfaces: the bigger waist to recouple, the more dependent it will be on alignment with the incident beam. This property is useful for all flat optics placed on the external benches and placed on setups using a millimeter-scale beam size: their recoupling by reflection will become negligible for very small misalignment.

In the following, we will use these calculated values of back reflected and back diffused light recoupling to project the associated displacement noise of the meniscus lens on the interferometer sensitivity using the formalism presented in section 2.1.

3.3. Noise projection on AdV sensitivity

Stray light from the telescope meniscus lens may spoil the interferometer sensitivity. The calculation carried out in the previous section showed that this noise will be dominated by back

#186188 - $15.00 USD Received 28 Feb 2013; revised 5 Apr 2013; accepted 5 Apr 2013; published 23 Apr 2013

reflection of the second surface of the meniscus lens with a recoupling of f_{sp2}=5.2.10^{-10}. Calculation of displacement noise introduced by the meniscus lens will therefore take into account only back reflection.

To make the noise projection on the AdV sensitivity curve, we have to make an estimation of the telescope optics horizontal motion. For this purpose, we have used an upper limit of ground seismic motion in case of high micro-seismic activity as presented in [30]. This noise was filtered to take into account the effect of the super-attenuator. The low frequency ground motion has been filtered by a factor of 100 between 0.1Hz and 1Hz as one can expect from the performances of Virgo super-attenuator inertial damping system [31]. The suspension chain also filters out the horizontal noise using the working principle of a pendulum that is filtering the noise above its cut-off frequency. Thus, the linear spectral density of the suspension point displacement decreases following the law $1/f^{2n}$ where n is the number of attenuation stages [32]. The Virgo super-attenuator has been designed to start to filter out the noise above a few Hz. So in our model, we used 1Hz as the cut-off frequency. In Fig. 9, the spectral density of the estimated upper limit of horizontal displacement of the optics installed on a suspended bench is shown. We considered having 3 stages of horizontal filtering thus the slope of the filter above

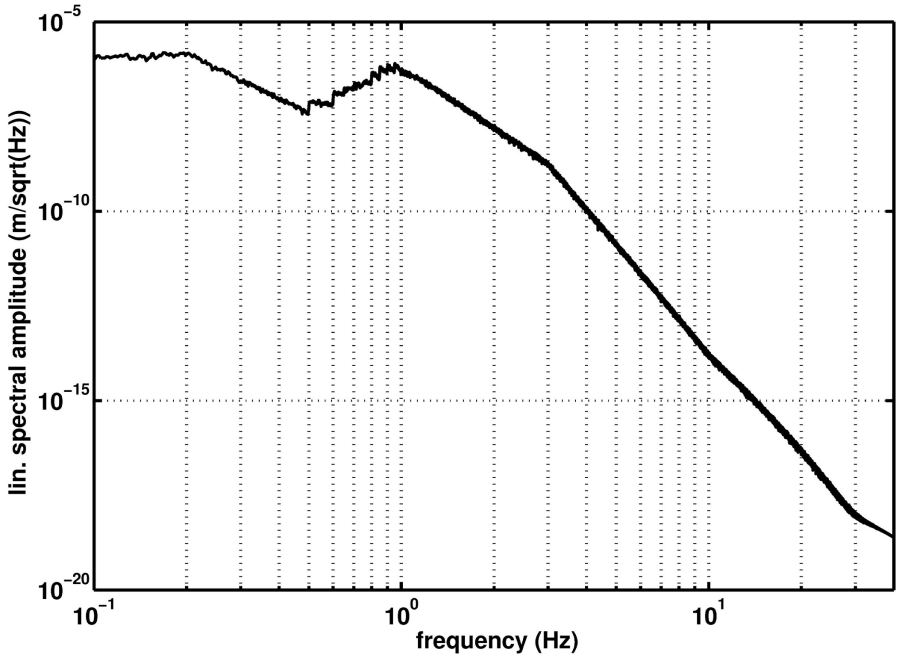

Fig. 9. Upper limit of horizontal displacement of the optics placed on the suspended bench.

the cut-off frequency follows $1/f^6$.

To make the noise projection, we used Eq. (7), Eq. (8) and the transfer function between phase noise and h and amplitude noise and h given in Fig. 1. In this case, we have not considered any asymmetries of the interferometer but all the work presented here can be easily redone considering ITF asymmetries by just recomputing the transfer function as explained in section 2.1. We have also considered that the laser power incident on the ITF is P_{in}=125 W and the power reflected by the ITF P_r is 20% of the incident power P_{in}. The projection of noise coming from stray light from INJ telescope optics on AdV sensitivity curve is given on Fig. 10.

As it can be seen in the noise projection given in Fig. 10, the amplitude noise is the most wor-

#186188 - $15.00 USD Received 28 Feb 2013; revised 5 Apr 2013; accepted 5 Apr 2013; published 23 Apr 2013

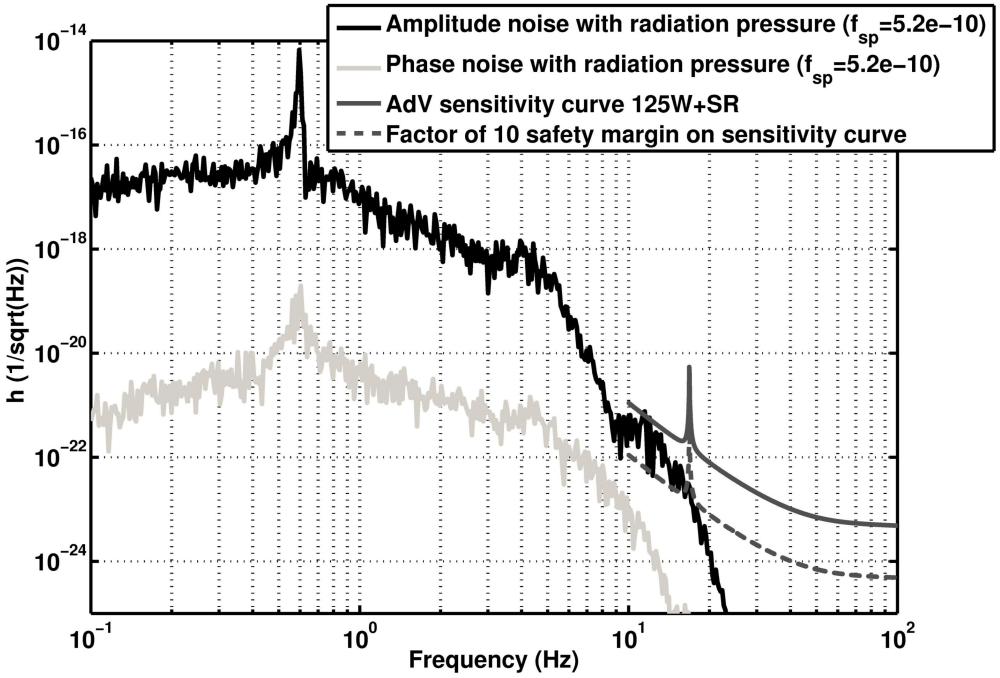

Fig. 10. Projection of the meniscus displacement noise in the worst conditions compared with AdV sensitivity.

risome noise coming from the input port. Indeed, in the worst ground seismic conditions, which are plausible for less than 5% of the time, the sensitivity may be limited at 10Hz by stray light coming from the meniscus lens. Therefore particular care will have to be taken with the suspension system of the benches to be sure that this system is working with optimal performance and in particular that all the low frequency resonances are properly damped and controlled. As explained in sections 3.1 and 3.2, the quality of the anti-reflective coating deposited on the meniscus lens surfaces is also particularly important since this is reducing the amount of light coming from back-reflected and back-scattered light recoupled in the interferometer. In the present work, we presumed a coating reflectivity lower than 100ppm that is already close to the best that can be achieved. For what concerns the phase noise, on Fig. 10 we see that it is expected to be a factor of 10 smaller than the amplitude noise. Moreover, in the interferometer standard operational mode, the phase noise coming from the interferometer input port is canceled out by a frequency stabilization loop [18] and in consequence we can reduce by several orders of magnitude the phase noise projection on AdV sensitivity.

Finally, particular care should be taken designing the optical benches located at the other exit ports of the interferometer (dark port, end station ports) that have demonstrated to be the most critical ones in the first generation of detectors. The formalism presented in this paper could be used to compute in the same way the contribution of those ports to the Advanced detectors noise budget.

4. Conclusion

In summary, we have discussed how the stray light originating from auxiliary optics is a challenging issue for Advanced GW detectors for achieving target sensitivity at low frequency. This

#186188 - $15.00 USD Received 28 Feb 2013; revised 5 Apr 2013; accepted 5 Apr 2013; published 23 Apr 2013

issue has to be taken into account at the design phase of these instruments as optics have limited performance in term of scattering and Anti-Reflective coating. We have proposed a complete formalism to calculate the displacement noise induced by the stray light originating from any optics, and applied this formalism to one of the critical components of AdV. We believe that other optical components at other ports could be even more critical. In such a case, if neither the optical setup can be changed, nor the optical performance of such a component can be improved, the control of the low frequency relative motion between the interferometer and the critical optical component should be further improved.

Acknowledgments

The research activity of one of the authors (G.Vajente) has been partially supported by Regione Toscana (Italy) through the program POR CreO FSE 2007-2013 of the European Community, within the project n. 18113 (ISAV).

#186188 - $15.00 USD Received 28 Feb 2013; revised 5 Apr 2013; accepted 5 Apr 2013; published 23 Apr 2013